J Mater Sci: Mater Med (2010) 21:131–137
DOI 10.1007/s10856-009-3857-3

Biomorphous porous hydroxyapatite-ceramics from rattan (*Calamus Rotang*)

Christiane Eichenseer · Julia Will · Markus Rampf · Süsen Wend · Peter Greil

Received: 23 April 2009 / Accepted: 13 August 2009 / Published online: 23 August 2009

Abstract The three-dimensional, highly oriented pore channel anatomy of native rattan (*Calamus rotang*) was used as a template to fabricate biomorphous hydroxyapatite ($Ca_5(PO_4)_3OH$) ceramics designed for bone regeneration scaffolds. A low viscous hydroxyapatite-sol was prepared from triethyl phosphite and calcium nitrate tetrahydrate and repeatedly vacuum infiltrated into the native template. The template was subsequently pyrolysed at 800°C to form a biocarbon replica of the native tissue. Heat treatment at 1,300°C in air atmosphere caused oxidation of the carbon skeleton and sintering of the hydroxyapatite. SEM analysis confirmed detailed replication of rattan anatomy. Porosity of the samples measured by mercury porosimetry showed a multimodal pore size distribution in the range of 300 nm to 300 µm. Phase composition was determined by XRD and FT-IR revealing hydroxyapatite as the dominant phase with minimum fractions of CaO and $Ca_3(PO_4)_2$. The biomorphous scaffolds with a total porosity of 70–80% obtained a compressive strength of 3–5 MPa in axial direction and 1–2 MPa in radial direction of the pore channel orientation. Bending strength was determined in a coaxial double ring test resulting in a maximum bending strength of ~2 MPa.

1 Introduction

An increasing interest in the development of synthetic porous hydroxyapatite (HA) as a bone replacement material is caused by limited supply of autograft material and the health risks associated with the use of allografts [1]. Porous scaffolds for bone tissue engineering should exhibit mechanical properties similar to that of bone and meet certain criteria such as osseoinductivity and tailorable biodegradation [2, 3]. Porous hydroxyapatite ceramics were reported to show bioactivity and to induce bone-like apatite formation (e.g. carbonated hydroxyapatite) in vitro when exposed to simulated body fluid (SBF) [1, 4–7]. Thus, the implant may trigger accelerated healing and direct implant-to-bone bonding is facilitated [1]. High porosity and large pores enhance bone ingrowth and osseointegration of the scaffold once implanted in the body [8]. According to early work of Hubert et al. [9] the minimum pore size for a scaffold should exceed 100 µm. Subsequent studies have shown even more effective osseogenesis for pore sizes >300 µm due to accelerated vascularization and oxygenation [8]. Over the past two decades many techniques have been developed to fabricate porous hydroxyapatite including polymeric sponge method [10], rapid prototyping techniques [11, 12], electrospinning [13], phase separation [14], particulate leaching [15], sacrificial filler [16], freeze casting [17], or gel-casting techniques [18]. Recently special attention has been paid to cellular scaffolds originating from biological tissue and materials like coral [19], cuttlefish [20], or bovine bone [21]. The aim of using biological structures as a template is to mimic natural structure hierarchy and anatomy at length scales covering a wide range from mm to nm [22]. The tissue of higher plants such as wood exhibits a hierarchical organisation of cells forming the vascular transportation system [3]. The honeycomb like microstructures of elongated hollow tubes may well be used for infiltration of liquid or gaseous reactants into the template. As described in literature, two different processes were developed to convert a template into a ceramic product: In the

C. Eichenseer · J. Will (✉) · M. Rampf · S. Wend · P. Greil
Department of Materials Science (Glass and Ceramics), University of Erlangen-Nuremberg, Henkestr. 91, 91052 Erlangen, Germany
e-mail: Julia.will@ww.uni-erlangen.de

transformation process natural wood was pyrolysed to obtain biocarbon templates which were infiltrated with a metal melt or vapour and subsequently reacted to form carbide phases (SiC, TiC) [23, 24]. In the substitution process, native or pyrolysed wood templates were infiltrated with precursor solutions of inorganic salts or metal organic precursors. The carbon skeleton was removed by high temperature oxidation leaving an oxide replica of the template structure (Al_2O_3, ZrO_2, TiO_2, MnO) [25, 26]. In this work, highly porous hydroxyapatite scaffolds for bone tissue engineering were prepared from a natural plant tissue. Rattan plants of the subfamily *Calamoideae* of the family *Arecaceae* offer a pore channel pattern with a unique multimodal pore size distribution. Typical cell diameters range from ~50 nm to ~50 μm with long continuous pores (metaxylem vessels) up to 400 μm in diameter. The porosity structure of these scaffolds is similar to the anatomy of cortical bone with a porosity of 55–70% [27]. Thus, mimicking the plant anatomy offers an interesting potential for regeneration of cortical bone tissue.

2 Experimental

2.1 Hydroxyapatite sol synthesis

A sol was prepared from triethyl phosphite ($P(OC_2H_5)_3$, 97%, Fluka Chemie GmbH, Buchs, Swiss) and calcium nitrate tetrahydrate ($Ca(NO_3)_2{\cdot}4H_2O$, ≥99%, Merck KGaA, Darmstadt, Germany) in ethanol/water solution. The molar ratio of water to the phosphorous precursor was kept at 8 for complete hydrolysis and the stoichiometric amount of the calcium to the phosphorous precursor at 1.67, respectively. The solution was allowed to age for 2 h at 60°C until a clear sol was obtained.

2.2 Template infiltration

Figure 1 shows the processing scheme applied. Cylindrical pieces of rattan (*Calamus rotang*) with a diameter of ~4 mm were dissected from internode sections of the stem. The pieces were cut into disks of 5–10 mm thickness and dried for 24 h at 105°C. The rattan samples were extracted with a mixture of toluol and ethanol at a volume ratio of 2:1 in a Soxhlet apparatus for 17 h to remove low-molecular weight species. Subsequently, samples were dried for 24 h at 105°C followed by a second extraction for 19 h using ethanol as solvent. After boiling the samples in distilled water for several hours a final drying for 24 h was proceeded at 105°C. For infiltration, the extracted samples were immersed in an evacuated glass beaker containing the hydroxyapatite-sol. After infiltration the samples were

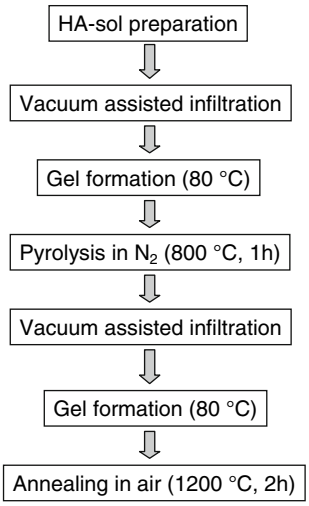

Fig. 1 Flow chart for the preparation of porous hydroxyapatite ceramics via biotemplating from rattan plants

dried for several hours at 80°C allowing the sol in the samples to form a hydroxyapatite-gel. This procedure was repeated up to 3 times. The samples were pyrolysed at 800°C for 1 h in N_2-atmosphere. During pyrolysis the biopolymers (cellulose, polyoses and lignin) were decomposed leaving a porous carbon residue covered with poorly crystalline hydroxyapatite. Multiple infiltration processes were carried out to increase the hydroxyapatite content. Finally, the specimens were annealed up to 1,300°C in air to remove the carbon template by oxidation and to transform the sol–gel into crystalline hydroxyapatite.

2.3 Sample characterization

Microstructure and morphology of native rattan templates and template-derived HA-scaffolds were examined by SEM (Quanta 200, FEI, Eindhoven/Netherlands). For SEM-imaging the samples were mounted on sample carriers using conductive carbon cement (Wetzlar/Germany) and sputtered with gold. Observation by SEM was carried out in ultra high vacuum with an accelerating voltage of 10 kV. Pore size distribution was analysed by means of mercury intrusion porosimetry (Hg-Porosimeter 2000, Carlo Erba Instruments, Milan/Italy) assuming a spherical pore geometry. For reference, porosity of HA scaffolds was determined from the relative density which was calculated from the apparent density of the sample divided by the theoretical density of hydroxyapatite (3.156 g/cm^3).

Chemical composition and crystalline phase content were analysed by XRD (Kristalloflex D500, Siemens, Karlsruhe/Germany) and FT-IR (Nicolet Impact 420, Nicolet Instruments, Madison/USA). Monochromated Cu-Kα radiation ($\lambda = 0.014505$ nm, 30 kV, 30 mA) was applied for XRD of powdered samples. The crystalline

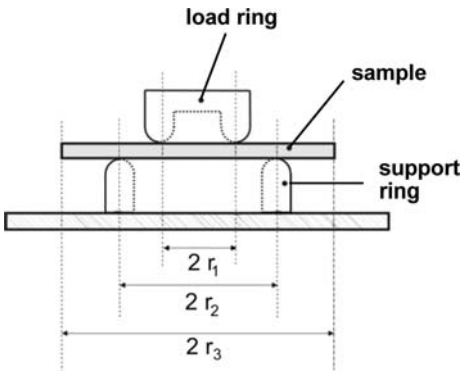

Fig. 2 Scheme of the double ring bending test arrangement

phases were identified according to the JCPDF files (HA: 09-0432, CaO: 37-1497, CHA: 19-272, β-TCP: 09-0169, α-TCP: 9-348 und TeCP: 25-1137). FT-IR-spectra were recorded in the range of 400–4,000 cm^{-1} in transmission mode with a resolution of 1 cm^{-1} using KBr technique. 1 mg of the sample powder was mixed with 300 mg KBr, grinded in a mortar and axially pressed into a transparent tablet.

The compressive and bending strengths of the porous hydroxyapatite scaffolds were measured (Instron 4204, Instron Corp., Canton/USA). Rectangular blocks with dimensions of $\sim 4 \times 4 \times 7$ mm^3 were machined for compressive loading according to DIN V ENV 1291 at a crosshead speed of 1.0 mm/min. Samples were loaded in axial (*out-of-plane*) and radial (*in-plane*) directions of the pore channel orientation. A minimum of eight samples was tested to derive an average value of compressive strength. Bending strength was obtained from cylindrical disk specimen with diameters of $\sim$30–40 mm and a height of $\sim$5 mm. Coaxial double ring test (DIN 52 292, Fig. 2) was performed with a radius ratio of load ring to support ring of r_1: $r_2 = 4$ and a crosshead speed of 0.5 mm/min.

3 Results and discussion

3.1 Pore structure

Figure 3 shows the structure and morphology of the rattan-derived hydroxyapatite ceramic sintered at 1,300°C as an exact replication of the native rattan tissue. Metaxylem vessels in the HA with diameters of (289 ± 15) µm are smaller than in the rattan template (379 ± 24) µm because of shrinkage during pyrolysis and sintering. Smaller phloem and protoxylem tracheids surrounding the large diameter metaxylem channels are well reproduced in the ceramic product and remained open. The grain size of HA sintered at 1,300°C ranges from 0.5 to 1.0 µm as determined from SEM micrographs. According to the results from mercury porosimetry, native rattan reveals lowest porosity of $\sim$55%, in comparison to HA ceramic with values of $\sim$60% and carbon template of $\sim$68%. Porosities calculated from relative density (determined through geometrical dimensions) attain slightly higher values of 76% for native rattan, 78% for HA and 83% for biocarbon template. Pore size distributions of native rattan, pyrolysed rattan and biomorphous HA ceramics are shown in Fig. 4. A three-modal pore size distrubution can be detected for all samples: nanopores with pore sizes in the range of 10–100 nm refer to cell wall pores; pores with diameters of 10–100 µm correspond to the trachaidal cell lumae. The third class of pores in the range of 200–400 µm displays large xylem vessels in the template. After conversion into HA ceramic the class of smallest pores shows a broader distribution in size in the range of 300 nm to 8 µm than in native or pyrolysed rattan. Peaks in the range of 10–100 µm and $\sim$200 µm can also be revealed in the HA ceramic which exhibits a similar three-modal pore size distribution as in the rattan template. Pore size distribution and porosity of HA ceramics lie within the range of spongy bone with pores from 200 to 400 µm in diameter and porosities of 55–70% [27, 28].

3.2 Phase composition

Figure 5 shows the FT-IR spectra of the rattan-derived hydroxyapatite scaffold sintered at 800–1,300°C. The main characterisitic bands of PO_4^{3-} together with characteristic modes of O–H groups confirm the presence of HA ($Ca_{10}(PO_4)_6(OH)_2$) in the reaction product. The peaks present at 567 and 604 cm^{-1} correspond to the v_4 fundamental vibrational mode and arise from bending vibrations of the PO_4^{3-} ions. The peak at 960 cm^{-1} is due to P–O symmetric stretching modes and is designated as the v_1 fundamental vibrational mode. Peaks at 1,036 and 1,086 cm^{-1} arise from the v_3 fundamental vibrational mode and are due to the asymmetric stretching modes of the P–O bonds [29, 30]. The sharp absorption bands at 875, 1,420 and 1,460 cm^{-1} in the spectra sintered at temperatures of 800–900°C also indicate the presence of CO_3^{2-} ions but disappear in the spectra of samples sintered at higher temperatures [2]. XRD patterns (Fig. 6) show identical peaks to the characteristic patterns of stoichiometric HA (JCPDF 09-0432). Small fractions of CaO are indicated by the presence of relevant peaks (JCPDF 048-1467) in all of the samples. Additional peaks are due to small amounts of β-TCP ($Ca_3(PO_4)_2$, JCPDF 09-0169) at lower temperatures from 800°C to 1,100°C and α-TCP (JCPDF 09-0348) at higher temperatures of 1,200–1,300°C. However, no characteristic bands of β-TCP at 1,118 and 945 cm^{-1} were observed in the FT-IR spectra. According to literature, the presence of β-TCP at

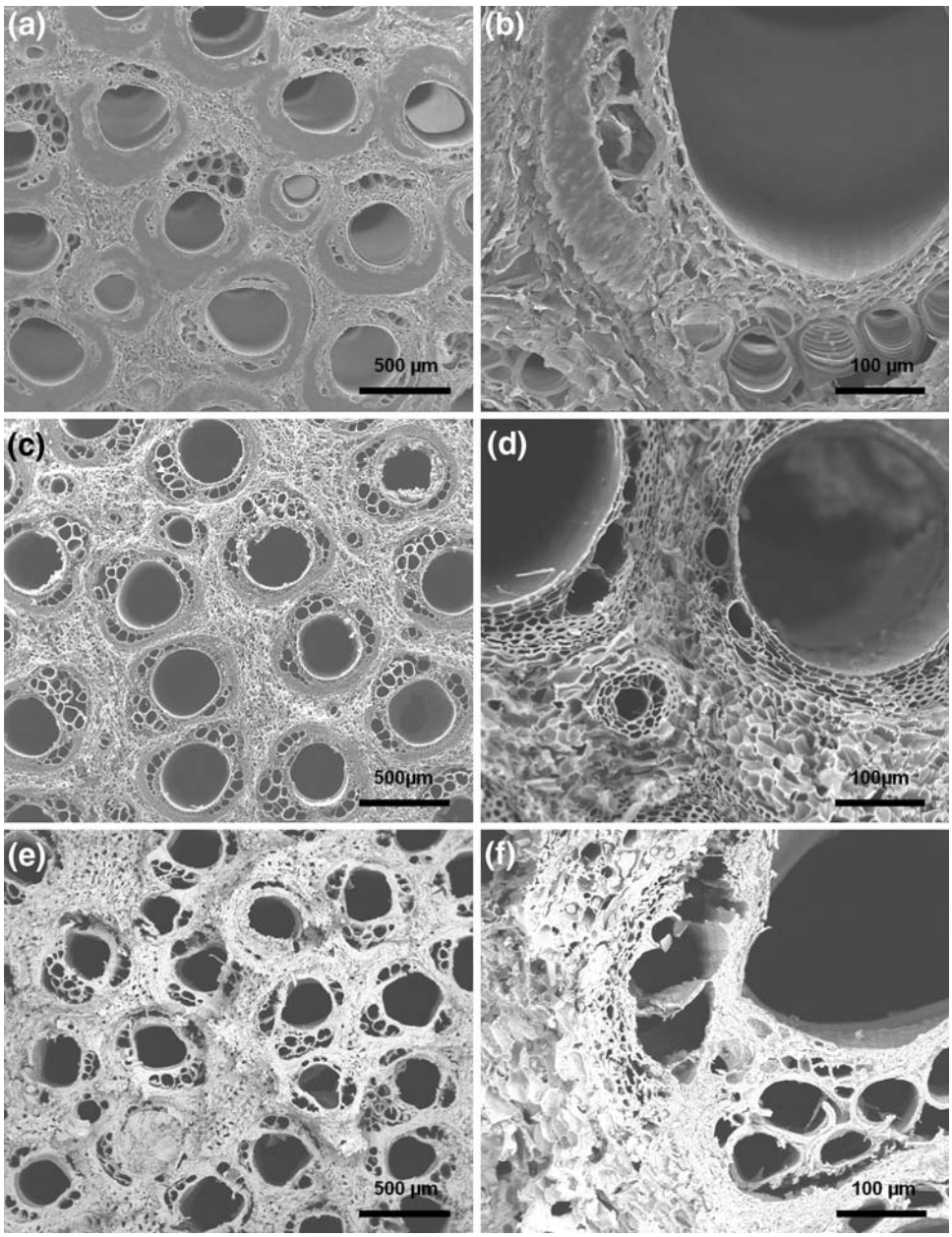

Fig. 3 SEM micrographs of native rattan (**a**, **b**), pyrolysed rattan (**c**, **d**) and biomorphous rattan-derived hydroxyapatite obtained at 1,300°C (**e**, **f**). Image planes show cross-sections perpendicular to axial stem direction

temperatures above 700°C is due to thermal decomposition of non-stoichiometric or carbonated hydroxyapatite [31, 32]. At temperatures above 1,150°C, β-TCP transforms into α-TCP [33]. CaO is the major impurity in sol–gel-derived hydroxyapatite [3] which is caused by insufficient aging of the precursor components mixture [34]. Calcium phosphates containing CaO are known to be biocompatible and bioresorbable [1, 35].

3.3 Strength and porosity

Figure 7 shows the compressive strength (*out-of-plane* loading) versus sintering temperature of the rattan-derived HA ceramics. A slight increase in fracture stress from (3.02 ± 0.53) MPa to (5.08 ± 1.66) MPa was observed with increasing sintering temperature from 800°C to 1,200°C. The biotemplated HA products exhibit porosity levels of 77–80%. Compared to human cancellous bone, which is characterized by a compressive strength of 5 MPa at porosities of 55–70%, the rattan derived biomorphous HA ceramics display similar strength levels when loaded along the pore channels [27]. Loading in radial direction, i.e. perpendicular to pore channels, however, revealed significantly lower values of (1.93 ± 0.85) MPa for samples sintered at 1,300°C.

Due to the similarity of pore channel morphology the mechanical behaviour of rattan derived ceramics may be described in analogy to honeycomb mechanics of brittle

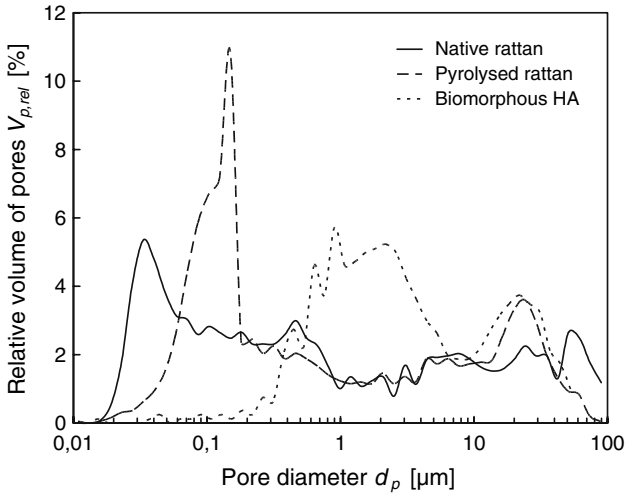

Fig. 4 Distribution of pore size versus relative volume of pores obtained from mercury intrusion porosimetry for rattan, pyrolysed rattan and rattan-derived hydroxyapatite

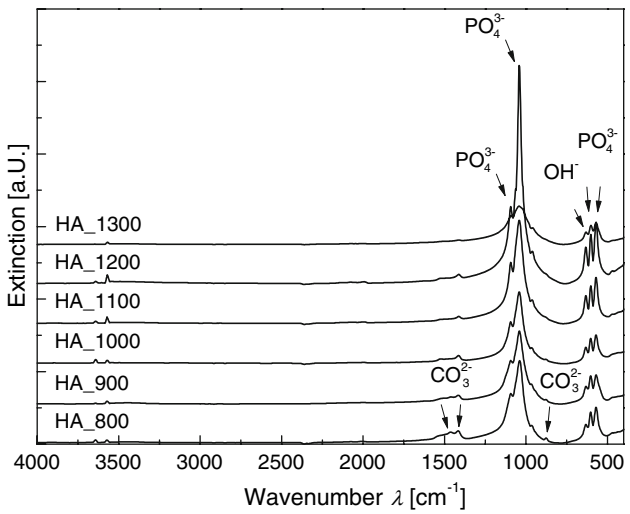

Fig. 5 FT-IR spectra of biomorphous HA-ceramics sintered at temperatures from 800°C to 1,300°C for 2 h

materials. In compression loading the cells suffer progressive crushing and in tension the pore channel structure fails by brittle fracture. For *in-plane* ($_{ip}$) compression loading e.g. loading stress acting perpendicular to the cell elongation, and for *out-of-plane* ($_{op}$) compression loading the fractional strength expressed by the ratio of crushing strength σ^*_{cr} to the failure strength of the strut material σ_{fs} is approximated by [36]

$$\frac{(\sigma^*_{cr})_{ip}}{\sigma_{fs}} = \frac{4}{9}\left(\frac{t}{l}\right)^2 \quad \text{and} \quad \frac{(\sigma^*_{cr})_{op}}{\sigma_{fs}} = 12\left(\frac{t}{l}\right) \tag{1}$$

Equation 1 was derived for regular hexagonal cell morphology characterized by a strut thickness t and a strut length l (circumference 6 l). Since in the naturally

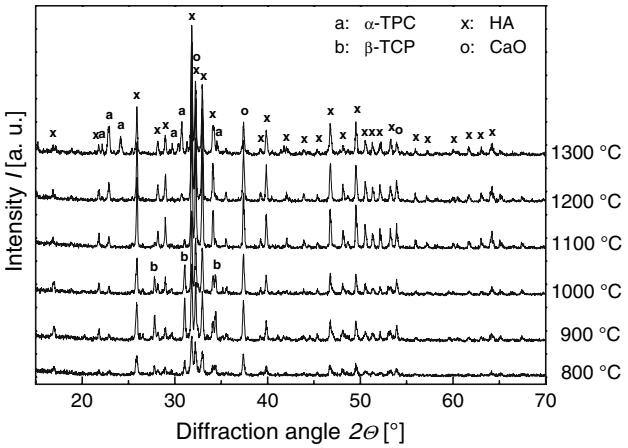

Fig. 6 XRD patterns of biomorphous HA ceramics sintered at temperatures from 800°C to 1,300°C for 2 h

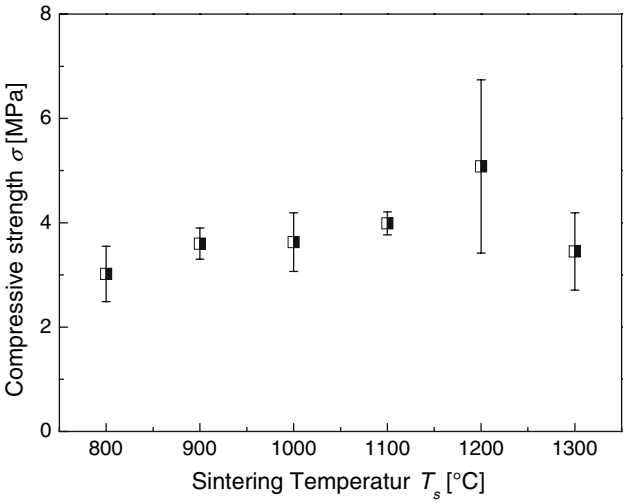

Fig. 7 Out-of-plane compressive strength versus sintering temperature of biomorphous HA-ceramics

grown tissue neither strut thickness t nor lumae dimension (l) remain constant but may locally vary significantly according to the seasonal growth conditions [37] the fracture stress as well as the other mechanical properties (Young's modulus, toughness) will vary in a periodical manner at least in the radial direction (seasonal growth direction). Even though Eq. 1 is a simplified approximation which does not take into account variation of t and l and the non-regular cell morphologies it can be used to estimate fracture properties of the strut material from the experimentally measured strength values. Approximating cylindrical cell morphology observed in rattan tissue by substituting $l \approx (\pi/3)r$ where r is the cylindrical pore channel radius the failure stress of the strut material is derived from

$$\sigma_{fs} \approx \frac{\pi}{36}\left(\frac{r}{t}\right)(\sigma^*_{cr})_{op} \tag{2}$$

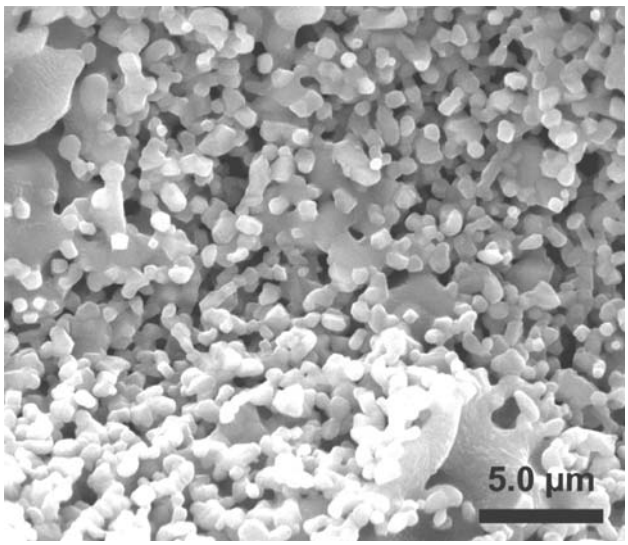

Fig. 8 SEM-micrograph of strut microstructure in porous HA-ceramic

for *out-of-plane* loading direction. Inserting experimental values for $(\sigma^*_{cr})_{op}$ shown in Fig. 7 and assuming a reasonable strut thickness of $t = 5$ µm a fracture stress of the struts σ_{fs} ranging from 2.1 to 21 MPa is derived for pore channel radii of 25 µm and 250 µm, respectively. These values are significantly lower compared to the data presented for hot-pressed HA of 560–700 MPa [29]. According to the common relations of strength and porosity of open cell foams [36] $\sigma^*_{cr}/\sigma_{fs} \approx 0.2(\rho^*/\rho_s)^{3/2}$a porosity of 0.7–0.93 of the strut material would result in such low compression strength values. SEM micrograph analysis of a typical strut microstructure in the sintered HA, Fig. 8, however, indicates the porosity in the sintered struts to be less than 0.5. Regular development of intercellular spaces between stegmata and parenchyma cells may give rise for the formation of pores and inhomogeneities in the struts which are likely to cause low fracture stresses [38]. Re-infiltration of the strut is a possible way to increase strut density and hence raise σ_{fs} to achieve higher loading capacity of biomorphous HA ceramics derived from natural rattan template.

4 Conclusions

Biomorphous hydroxyapatite-ceramics with a porosity of 70–80% were fabricated by sol infiltration of a rattan template. After repeating sol infiltration in the carbon template, annealing in air at 1,300°C resulted in oxidizing of the carbon and sintering of the hydroxyapatite ceramic. The cellular anatomy of the native tissue template with a three-modal pore size distribution was transferred into HA ceramics. Despite of a high porosity, the HA scaffold achieved sufficient mechanical strength to serve as spongious bone implants. Biomorphous HA ceramics fabricated in this study exhibit properties very similar to human cancellous bone in terms of porosity, pore size and mechanical stability.

Acknowledgement The authors greatfully acknowledge the EU commission for the financial support under the FP6 number NMP4-CT-2006-033277.

References

1. Hing KA, Best SM, Bonfield W. Characterization of porous hydroxyapatite. J Mater Sci: Mater Med. 1999;10:135–45.
2. Krajewski A, Mazzocchi M, Buldini PL, Ravaglioli A, Tinti A, Taddei P, et al. Synthesis of carbonated hydroxyapatite: efficiency of the substitution and critical evaluation of analytical methods. J Mol Struct. 2005;744–747:221–8.
3. Qian J, Kang Y, Zhang W, Li Z. Fabrication, chemical composition change and phase evolution of biomorphic hydroxyapatite. J Mater Sci: Mater Med. 2008;19:3373–83.
4. LeGeros RZ. Apatites in biological systems. Prog Cryst Grow Char. 1981;4:1–45.
5. Hench LL. Bioceramics, from concept to clinic. J Am Ceram Soc. 1991;74:1487–510.
6. Tampieri A, Celotti G, Landi E, Montevecchi M, Roveri N, Bigi A, et al. Porous phosphate-gelatine composite as bone graft with drug delivery function. J Mater Sci: Mater Med. 2003;14:623–7.
7. Moura J, Teixeira LN, Ravagnani C, Peitl O, Zanotto ED, Beloti MM, et al. In vitro osteogenesis on a highly bioactive glass–ceramic (Biosilicate®). J Biomed Mater Res. 2007;82A:545–57.
8. Karageorgiou V, Kaplan D. Porosity of 3D biomaterial scaffolds and osteogenesis. Biomaterials. 2005;26:5474–91.
9. Hubert SF, Young FA, Mathews RS, Klawitter JJ, Talbert CD, Stelling FH. Potential of ceramic materials as permanently implantable skeletal protheses. J Biomed Mater Res. 1970;4:190–9.
10. Sopyan I, Kaur J, Toibah JAR, Hamdi M, Ramesh S. Effect of slurry preparation on physical properties of porous hydroxyapatite prepared via polymeric sponge method. Adv Mater Res. 2008;47–50:932–5.
11. Williams JM, Adewunmi A, Schek RM, Flanagan CL, Krebsbach PH, Feinberg SE, et al. Bone tissue engineering using polycaprolactone scaffolds fabricated via selective laser sintering. Biomaterials. 2005;26:4817–27.
12. Will J, Melcher R, Treul C, Travitzky N, Kneser U, Polykandriotis E, et al. Porous bone scaffolds for vascularized bone tissue regeneration. J Mater Sci: Mater Med. 2008;19:2781–90.
13. Kim H-W, Kim H-E, Knowles JC. Production and potential of bioactive glass nanofibers as a next-generation biomaterial. Adv Funct Mater. 2006;16:1529–35.
14. Helen W, Merry CLR, Blaker JJ, Gough JE. Three-dimensional culture of annulus fibrosus cells within PDLLA/Bioglass® composite foam scaffolds: assessment of cell attachment, proliferation and extracellular matrix production. Biomaterials. 2007;28:2010–20.
15. Tadic D, Beckmann F, Schwarz K, Epple M. A novel method to produce hydroxyapatite objects with interconnecting porosity that avoids sintering. Biomaterials. 2004;25:3335–40.
16. Vitale Brovarone C, Verné E, Appendino P. Macroporous bioactive glass–ceramic scaffolds for tissue engineering. J Mater Sci: Mater Med. 2006;17:1069–78.

17. Deville S, Saiz E, Tomsia AP. Freeze casting of hydroxyapatite scaffolds for bone tissue engineering. Biomaterials. 2006;27: 5480–9.
18. Ramay HR, Zhang M. Preparation of porous hydroxyapatite scaffolds by combination of the gel-casting and polymer sponge methods. Biomaterials. 2003;24:3293–302.
19. Murugan R, Panduranga RK, Sampath KTS. Microwave synthesis of bioresorbable carbonated hydroxyapatite using goniopora. Key Eng Mater. 2003;240–242:51–4.
20. Kannan S, Rocha JHG, Agathopolulos S, Ferreira JMF. Fluorine-substituted hydroxyapatite scaffolds hydrothermally grown from aragonitic cuttlefish bones. Acta Biomater. 2007;3:243.
21. Worth A, Mucalo M, Horne G, Bruce W, Burbidge H. The evaluation of processed cancellous bovine bone as a bone graft substitute. Clin Oral Implants Res. 2005;16:379–86.
22. Tampieri A, Sprio S, Ruffini A, Celotti G, Lesci G, Roveri N. From wood to bone: multi step-process to convert wood hierarchical structures into mimetic hydroxyapatite scaffolds for bone tissue engineering. J Mater Chem. 2009;19:4973–80.
23. Singh M, Martínez-Fernández J, de Arellano-López AR. Environmentally conscious ceramics (ecoceramics) from natural wood precursors. Curr Opinion Solid State Mater Sci. 2003;7:247–54.
24. Sieber H. Biomimetic synthesis of ceramics and ceramic composites. Mater Sci Eng A. 2005;412:43–7.
25. Cao J. Biotemplating of highly porous oxide ceramics. Göttingen/D: Cuvillier Verlag; 2005.
26. Rambo CR, Sieber H. Novel synthetic route to biomorphic Al_2O_3 ceramics. Adv Mater. 2005;17:1088–91.
27. Jones JR, Hench LL. Regeneration of trabecular bone using porous ceramics. Curr Opinion Solid State Mater Sci. 2003;7:301–7.
28. Hartung C. Zur Biomechanik weicher Gewebe. VDI Fortschrittsberichte. Reihe Biotechnik. 1975;17(2):91.
29. Rey C, Collins B, Goehl T, Dickson IR, Glimcher MJ. The carbonate environment in bone mineral: a resolution-enhanced Fourier transform infrared spectroscopy study. Calcif Tissue Int. 1989;45:157–64.
30. Koutsopoulos S. Synthesis and characterization of hydroxyapatite crystals: a review study on the analytical methods. J Biomed Mater Res A. 2002;62:600–12.
31. Liu D-M, Trczynski T, Tseng WJ. Water.based sol–gel synthesis of hydroxyapatite: üprocess development. Biomaterials. 2001;22:1721–30.
32. Lafon JP, Champion E, Bernache-Assollant D. Processing of AB-type carbonated hydroxyapatite $Ca_{10-x}(PO_4)_{6-x}(CO_3)_x(OH)_{2-x-2y}(CO_3)_y$ ceramics with controlled composition. J Eur Ceram Soc. 2008;28:139–47.
33. Welch JH, Gutt W. High-temperature studies of the system calcium oxide-phosphorus pentoxide. J Chem Soc. 1961;IV:4442–4.
34. Liu D-M, Troczynski T, Tseng WJ. Aging effect on the phase evolution of water-based sol–gel hydroxyapatite. Biomaterials. 2002;23:1227–36.
35. de Groot K, Klein CPAT, Wolke JGC, de Blieck Hogervorst JMA. Chemistry of calcium phosphate bioceramics. In: Yamamuro T, Hench LL, Wilson J, editors. CRC handbook of bioactive ceramics, calcium phosphate and hydroxyapatite ceramics, vol. II. Boca Raton, FL: CRC Press; 1990. p. 3–16.
36. Gibson LJ, Ashby MF. Cellular solids, structure and properties. New York: Pergammon Press; 1988.
37. Greil P. Biomorphous ceramics from lignocellulosics. J Eur Ceram Soc. 2001;21:105–18.
38. Schmitt G, Weiner U, Liese W. The fine structure of the stegmata in *Calamus Axillaris* during maturation. JAWA J. 1995;16:61–8.